*Jordan Journal of Pharmaceutical Sciences, Volume 13, No. 2, 2020*

# Discovery of Novel Glyoxalase-I Inhibitors Using Computational Fragment-Based Drug Design Approach

*Nizar A. Al-Shar'i[1], Mohammad A. Hassan[1], Hadil M. Al-Barqi[1], Qosay A. Al-Balas[1], and Tamam El-Elimat[1]**

1-Department of Medicinal Chemistry and Pharmacognosy, Faculty of Pharmacy, Jordan University of Science and Technology, Irbid, Jordan.

## ABSTRACT

In this study, a computational fragment-based drug design approach was employed to design potential glyoxalase-I (GLO-I) inhibitors. GLO-Iis overexpressed in various cancer types, which made it a viable target for cancer treatment. The current approach was based on screening the Maybridge Ro3 diversity fragment library using different computational techniques to select potential fragments that can be evoluted to putative drug-like active compounds. Six fragments were selected that are complementary to the main binding regions within the GLO-I active site. Fragments merging and linking had resulted in 21 potential GLO-I inhibitors. To assess the applicability of this approach, one pilot compound (**12**) was synthesized and biologically evaluated. The % of GLO-I inhibition by **12** at 50 $\mu$M was 44%,one fold lower than that of myricetin (86%) indicating that the utilized approach was successful. Despite the weak activity, the percent of inhibition of **12** can be extrapolated to get a rough estimate of the expected activities of other compounds within the evoluted set. Moreover, compound **12** could be considered as a new hit with a novel chemotype that can be further optimized towards designing more potent inhibitors.

**Keywords**: Glyoxalase-I, Fragment-Based Drug Design, Zinc binding, Anticancer.

## INTRODUCTION

The glyoxalase enzyme system is one of the detoxifying enzymes in the body and is composed of two consecutive enzymes, namely glyoxalase-I (GLO-I) and glyoxalase-II (GLO-II) that sequentially catalyzes the transformation of methylglyoxal (MG), a toxic metabolite, into nontoxic lactic acid [1]. Detoxification is achieved by isomerization of hemithioacetal, formed non-enzymatically from methylglyoxal and glutathione (GSH), by GLO-I enzyme into S-D-lactoylglutathione[2]. Then, GLO-II catalyzes the hydrolysis of S-D-lactoylglutathione to release D-lactic acid and regenerates GSH. MG is a highly reactive species with potential ability to react with DNA, RNA and proteins, subsequently causing cell damage [3]. Highly proliferating cells, such as tumor cells, have a high glycolytic activity which is associated with elevated concentrations of toxic metabolites such as MG. Tumor cells respond to this by increasing the expression and activity of the detoxifying glyoxalase system, particularly the GLO-I enzyme [2, 4]. Overexpression of GLO-I has been reported in various cancer types such as invasive ovarian cancer, breast cancer, human lung carcinoma, prostate carcinoma, and recently reported in melanoma [5-8], which made it an attractive target for many research groups [9-15]. However, up to date, there is no clinically approved drugs targeting the GLO-I enzyme, hence, more efforts are needed to achieve the desired inhibition.

Structurally, the human GLO-I enzyme is a homodimeric zinc metalloenzyme. Each monomer is made of 183 amino acids with a molecular weight of approximately 42 kDa. The active site of the enzyme is

*nashari@just.edu.jo

Received on 31/3/2019 and Accepted for Publication on 8/7/2019.

 

situated at the interface of the two chains, and the $Zn^{2+}$ ion is coordinated by four amino acids from both chains [16-18]. Beside the $Zn^{2+}$ binding region, the GLO-I active site can be divided into a hydrophobic pocket which is next to $Zn^{2+}$ and composed of Met-157B, Met-183B, Phe-67A, Phe-62B, Leu-160B and Lys-156B, and a hydrophilic positively charged mouth that is composed of two arginine amino acids namely, Arg-37A and Arg-122B (Figure 1).

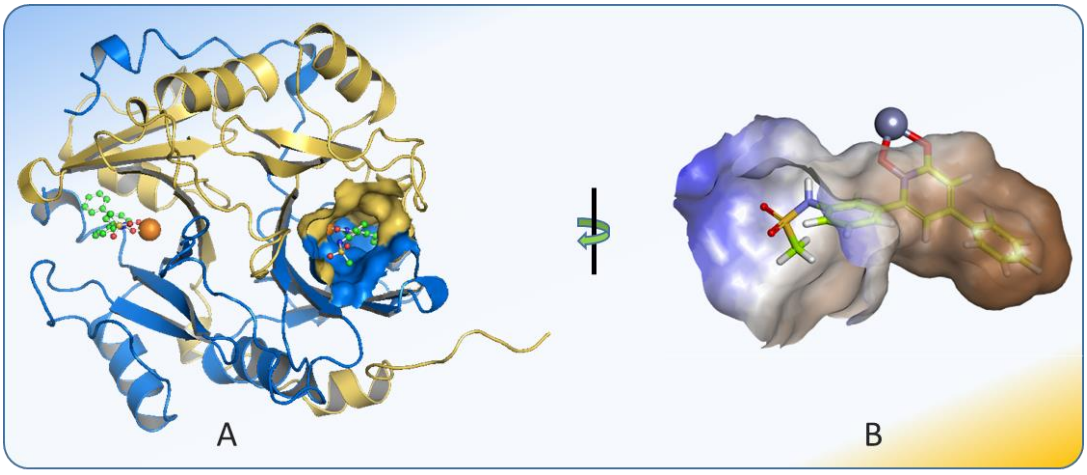


**Figure 1:** (A) Cartoon representation of the GLO-I enzyme (PDB code 3W0T). Chain A is in pale yellow and chain B is in blue, the complexed ligands are in ball and sticks, and $Zn^{2+}$ as an orange sphere. The active site is shown as a surface to highlight its location between the two chains. (B) A closer view of the active site represented as a hydrophobic surface to illustrate the three main binding regions. The $Zn^{2+}$ ion (purple), the hydrophobic pocket (brown), and the positively charged mouth (blue).

The GLO-I enzyme has been the focus of our research group where different approaches have been applied in which many compounds with diverse scaffolds have been designed, synthesized, and screened [13-15, 19]. In this study, computational fragment-based drug design (FBDD) approach was applied in an attempt to design potent GLO-I inhibitors with novel chemical scaffolds as potential anticancer agents. The fundamental components of the computational fragment-based design are a set of building blocks (fragment library), a construction process, an optimization procedure, and a scoring function. Moreover, good knowledge of the target binding site is invaluable in aiding the evolution of core fragments towards putative active ligands which can be achieved via either fragment growing, direct connection (merging or joining), or by fragments linking [10]. To this end, we utilized different protocols available in Discovery Studio [20] such as MCSS (Multiple Copy Simultaneous Search) docking, CDOCKER docking, flexible docking, and calculation of binding energy using MM-PBSA solvent model [21]. These protocols were used to screen Maybridge Ro3 fragment library [22] to aid the selection of core fragments that will eventually be evoluted to drug-like compounds that will be biologically evaluated.

## 1. MATERIALS AND METHODS

### 1.1 *Computational Materials*

Sketching of fragments and evoluted compounds was performed using ChemBioDraw Ultra 12.0. All

computational design steps were performed using Discovery Studio (DS) 2017 from Biovia Software Inc. (Accelrys Inc.: San Diego, CA, USA). Presentation quality images were generated using the PyMOL Molecular Graphics System [23] and DS. GraphPad Prism [24] was used for calculation of the % of GLO-I inhibition.

### 1.2 *Experimental Instrumentation and Materials*

NMR data were collected using a JEOL ECS-400 NMR spectrometer equipped with a high sensitivity JEOL Royal probe and a 24-slot autosampler (JEOL Ltd.) or a Bruker AvanceUltrashield spectrometer (Bruker Corp.), operating at 400 MHz for $^{1}$H and 100 MHz for $^{13}$C. Residual solvent signals were utilized for referencing. Infrared (IR) spectra were recorded on KBr pellets using Shimadzu IR Affinity-1 FTIR (Shimadzu Corp.). HRMS data were acquired using a ThermoQExactive Plus mass spectrometer equipped with an electrospray ionization source (Thermo Fisher Scientific). However, LRMS data were collected using Applied Biosystems MDS SCIEX API 3200 LC/MS/MS systemequipped with an electrospray ionization source(AB Sciex). Selected fragments were purchased from ACROS Chemicals, New Jersey, USA; and Combi-blocks, San Diego, USA.

### 1.3 Computational Methods

Generally, the computational approach of FBDD involves three basic steps, which are: (1) the design of a good fragment library; (2) computational docking, ranking or screening of the fragments library; (3) growing, linking or merging of fragments to yield the final drug-like compounds. The last two steps were performed within the binding site of the target protein; therefore, a prepared 3D structure of the target of interest was needed.

#### 1.3.1 Preparation of the GLO-I Enzyme

The structural model of the GLO-I enzyme was prepared using Discovery Studio (DS) 2017 from Biovia Software Inc. The initial coordinates for GLO-I were obtained from the Protein Data Bank. Six GLO-I crystal structures were available in the protein data bank with accession codes 3VW9, 3W0T, 3W0U, 1QIN, 1QIP, and 1FRO. The selected crystal structure was the one with the highest resolution (entry code 3W0T), which corresponds to GLO-I in complex with *N*-hydroxypyridone derivative inhibitor at 1.35 Å resolution. The PDB file was checked for missing loops, alternate conformations and incomplete residues using *Protein Report* tool within DS. Then, the structure was cleaned using the *Clean Protein* protocol to standardize atoms names, correct connectivity and bond order, and adding hydrogens at a pH of 7.4. Finally, the enzyme was typed using the *Simulation* tools by applying CHARMm force field [25].

#### 1.3.2 Fragment Library Design

The fragment library used in this research was the predesigned Maybridge Ro3 diversity fragment library, which contains 2,500 structurally diverse fragments. The library was downloaded, and then was imported into DS and prepared using the *Prepare Ligand* protocol within DS using default parameters. Correct and good preparation of ligands when studying receptor-ligand interactions is very important. This is due to the facts that different protonation states, isomers and tautomers typically have different 3D geometries and binding characteristics. Different tasks of ligand preparation can be performed using this protocol, such as standardizing charges for common groups, adding hydrogens, enumerating different ionization states, generating tautomers and isomers, fixing bad valencies, and calculating the 3D coordinates. Then, the prepared library was converted into a 3D database using the *Build 3D Database* protocol, which uses the *Catalyst*algorithm [26, 27]. The generated 3D database is automatically indexed with sub-structure, pharmacophore feature, and shape information to allow fast database searching.

**1.3.3 Fragment Docking and Scoring**

Prior to fragment docking, the GLO-I active site was defined using the *Define and Edit Binding Site* tool within DS into two regions, namely the zinc-hydrophobic pocket region and the positively charged mouth region. The zinc-hydrophobic pocket region, which is composed of the $Zn^{2+}$ ion, Met-157B, Met-183B, Phe-67A, Phe-62B, Leu-160B and Lys-156B, was defined by a sphere of 7 Å radius. The positively charged region, included Arg-37A and Arg-122B, was defined by a sphere of 9 Å radius. Then the *MCSS docking* protocol was employed using default parameters [28].

**1.3.4 Calculation of the Binding Energy of Docked Fragments**

The binding energy of the docked fragments in both specified docking regions was calculated using the *in Situ Ligand Minimization* and the *Calculate Binding Energies* protocols [29]. The *in situ* ligand minimization was performed using the Adopted Basis Newton-Raphson (NR) algorithm [30, 31]. The *Calculate Binding Energies* protocol was applied using default parameters except for the ligand conformation entropy which was set to true, and the implicit solvent system for which the Poisson Boltzmann with non-polar surface area (MM-PBSA) model [21] was selected.

**1.3.5 Ligand Efficiency of Docked Fragments**

Ligand efficiency (LE) was calculated for the top-ranked fragments in terms of binding energy using *Calculate Ligand Efficiency* protocol, using fragments with estimated binding energies as input ligands [32, 33].

**1.3.6 Fragment Evolution**

Different methods can be used to design drug-like compounds from smaller fragments such as: fragment growing, where a top binding fragment is considered as an anchor within the active site of the target, and then according to the empty pockets within the active site additional fragments would be added in a complimentary manner to end up with lead compounds with enhanced binding affinity. Fragment merging/hopping, where two or more fragments binding in different neighboring binding areas of the active site and overlapping with each other are merged to generate the final lead compound. Finally, fragment linking, where two fragments fitted in different areas of the active site are connected using a linker to obtain the final lead compound [10]. In this study, the top ranked fragments binding in both regions within the active site were evoluted using two fragment evolution strategies, fragment linking and fragment merging depending on the distance separating the two fragments.

**1.3.7 Molecular Docking and Calculation of Binding Energy of Evoluted Compounds**

Prior to molecular docking of the evoluted compounds, the GLO-I active site was defined using the *Define and Edit Binding Site* tool within DS by a sphere of 13 Å radius based on the complexed ligand. Afterwards, the evoluted compounds were docked into the GLO-I active site using CDOCKER docking protocol in DS using default parameters. Then, the binding energies of the docked poses were calculated using the *Calculate Binding Energies* protocol [29] after being minimized using the *In SituLigand Minimization* protocol using the same parameters used in calculating the binding energies of the docked fragments.

To get a better insight of the binding modes of the evoluted compounds they were redocked into the active site of the GLO-I enzyme using *Flexible Docking* protocol within DS. The *Flexible Docking* protocol was implemented using default parameters except for generate ligand conformation, which was set to "best". Amino acids corresponding to the GLO-I active site; namely Met157A, Phe162A, Met179A, Leu182A, Met183A, Arg122A, Met35B, Arg37B, Cys60B, Phe62B, and Leu69B were defined as the flexible group that will be allowed to move

during the docking process. A summary of the entire design approach implemented in this study is illustrated in figure 2.

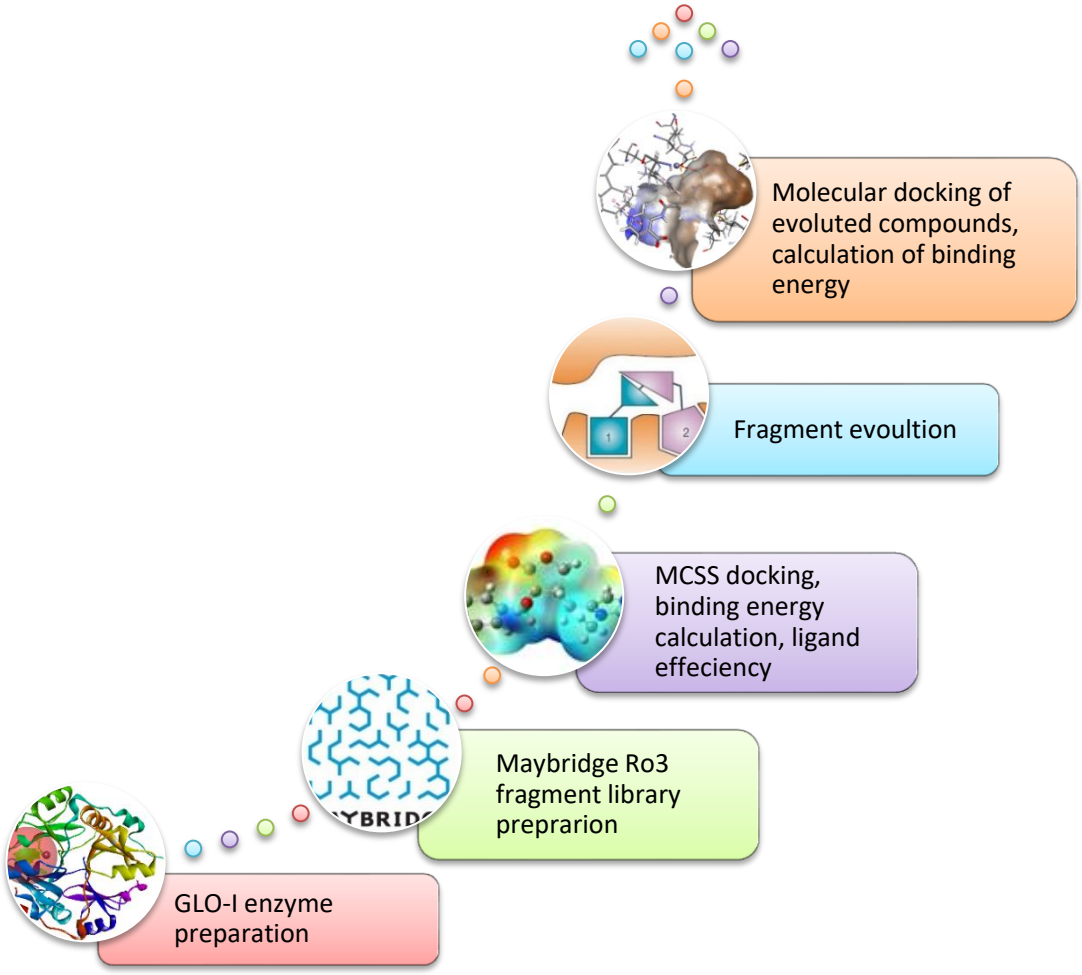


**Figure 2: General workflow of the employed design methodology.**

### 1.4 Experimental Methods

#### 1.4.1 Chemistry

Synthesis of the final evoluted compound was achieved via a four-step scheme, as detailed below, where the fragment binding the positively charged mouth was first coupled to the 3-nitrobenzoyl chloride linker. Then the linker's nitro group was reduced into an amino group, afterwards, the Zn-hydrophobic binding fragment was coupled to the linker via its amino group. Finally, the ester functionalities were hydrolyzed to afford the final desired compound.

***Synthesis of methyl 3-(3-nitrobenzamido)isonicotinate(1a)***

The methyl 3-aminoisonicotinate fragment, binding the positively charged mouth, (fragment 3B analogue) (13.15 mmol, 2.00 g) was reacted with 3-nitrobenzoyl chloride linker (13.15 mmol, 2.43 g) in tetrahydrofuran (THF) using pyridine as a base. The product has appeared quickly, once 3-nitrobenzoyl chloride was added a

precipitate started to form. The reaction took around 15 min to complete. Thin Layer Chromatography (TLC) was used to track the progress of product formation. Upon completion of the reaction, the reaction mixture was poured into acid water and left in fridge allowing the product to precipitate. Then, the reaction mixture was filtered, and 4.26 g of product was collected as yellow crystals (96.2% yield). The product was found to be pure enough and required no further purification. $^{1}$H NMR (400 MHz, DMSO-$d_6$): $\delta_H$3.84 (3H, s, $OCH_3$), 7.85 (1H, d, $J$ = 5.2 Hz, Ar-H), 7.90 (1H, t, $J$ = 8, Ar-H), 8.43 (1H, d, $J$ = 8, Ar-H), 8.50 (1H, d, $J$ = 8, Ar-H), 8.64 (1H, d, $J$ = 5.2, Ar-H), 8.79 (1H, s, Ar-H); 9.18 (1H, s, Ar-H), 11.32 (1H, s, CO-NH). $^{13}$C NMR (400 MHz, DMSO-$d_6$): $\delta_C$52.9, 122.4, 123.6, 123.7, 126.9, 130.7, 132.9, 133.9, 134.9, 144.6, 144.9, 148.0, 163.6, 165.5.

***Synthesis of methyl 3-(3-aminobenzamido)isonicotinate (1b)***

Compound **1a** (12.61 mmol, 3.8 g) was dissolved in methanol and a catalytic amount of Pd/C was added, all in well-sealed round bottom flask where a long needle was inserted and allowed to immerse into the reaction solution to facilitate hydrogen gas to bubble within the solution and reduce the nitro into an amino group [34]. The reaction progress was checked by TLC and was left overnight for completion. Afterwards, the reaction mixture was filtered using suction filtration, filtrate was concentrated *in vacuum*, and the product was recrystallized using methanol and chloroform to obtain 1.9 g of yellow crystals (50% yield). IR $\nu_{max}$ 1653, 1732 and 3370 cm$^{-1}$.

***Synthesis of methyl 3-(3-((2-methoxy-2-oxo-1-phenylethyl)amino)benzamido) (1c)***

Compound **1b** (1.1 mmol, 0.3 g) was reacted with methyl 2-bromo-2-phenylacetate (fragment 2A analogue) (1.1 mmol, 0.25 g) in THF with one equivalent of potassium carbonate at room temperature. The reaction progress was checked by TLC and was left overnight for completion, then poured in ice water and put in fridge for product to precipitate. Formed product was collected and recrystallized from ethyl acetate and hexane to obtain 0.018 g of yellowish white crystals (4% yield). $^{1}$H NMR (400 MHz, $CDCl_3$): $\delta_H$ 3.69 (3H, s, $OCH_3$), 3.95 (3H, s, $OCH_3$), 5.12 (1H, s, -CH-), 6.67 (1H, d, $J$ = 8 Hz, Ar-H), 7.17-7.46 (7H, Aromatic), 7.78 (1H, dd, $J$ = 5.2, Ar-H), 8.34 (1H, d, $J$ = 5.2, Ar-H), 10.14 (1H, s, Ar-H), 11.41 (1H, s, CO-NH). $^{13}$C NMR (100 MHz, $CDCl_3$): $\delta_C$ 53.1, 53.3, 60.6, 112.7, 116.6, 117.4, 121.2, 122.9, 127.4, 127.4, 128.6, 129.1, 129.1, 129.9, 135.2, 136.9, 137.2, 143.7, 146.7, 146.5, 165.8, 167.7, 172.2.

***Hydrolysis of methyl 3-(3-((2-methoxy-2-oxo-1-phenylethyl)amino)benzamido) isonicotinate*to obtain the final evoluted compound (12)**

The final compound (number **12** in table 3) was obtained by hydrolyzing compound **1c**. Compound **1c** (0.0429 mmol, 0.018 g) was added to a solution of 30 mL of 0.3 mM sodium hydroxide and ethanol (1:1). The mixture was heated under reflux for 30 min. Then, the pH of the mixture was adjusted to 3.0 using 1 M HCl and the mixture was left in a refrigerator overnight. The precipitated compound was collected and recrystallized from methanol and dichloromethane to obtain 0.007 g of yellowish white crystals (36% yield). IR $\nu_{max}$ 1604, 1726, 3064 and 3370 cm$^{-1}$. $^{1}$H NMR (400 MHz, $CD_3OD$): $\delta_H$ 5.11 (1H, s, -CH-); 6.79 (H, d, $J$ = 6.4 Hz, Ar-H); 7.20-7.59 (7H, Aromatic); 7.99 (1H, d, $J$ = 3.6, Ar-H); 8.29 (1H, d, $J$ = 3.6, Ar-H); 9.93 (1H, s, Ar-H). $^{13}$C NMR (100 MHz, CD3OD): $\delta_C$ 62.5, 113.6, 117.0, 117.6, 119.9, 128.7, 128.7, 128.9, 129.6, 129.6, 130.5, 130.6, 136.3, 136.4, 138.2, 142.2, 144.0, 148.9, 168.0, 171.7, 173.7. HRESIMS $m/z$: 390.1094 (M-H$^-$) (calcd for $C_{21}H_{16}N_3O_5$ 390.1095).

### 1.4.2 In vitro enzyme assay

The inhibitory activity of the synthesized compound was performed *in vitro* using the human recombinant Glo-I (rhGlo-I) as detailed elsewhere [14, 15].

## 2. RESULTS AND DISCUSSION

### 2.1 *In silico drug design*

The binding site of GLO-I is divided into three regions as mentioned previously. However, for the purpose of applying FBDD strategy and because the zinc atom is very close to the hydrophobic pocket, the binding site was divided into two regions, the Zn-hydrophobic region and the positively charged mouth region.

#### 2.1.1 Fragment Library Design

The design of a fragment library is a very crucial step in FBDD. The properties of a good fragment library are diversity of physicochemical properties, molecular diversity, aqueous solubility, and drug-likeness [35]. A set of rules, referred to as the "rule of three", has been proposed to aid the selection of fragments comprising a library. The rule of three entails the following parameters: molecular weight less than or equal 300 Da, LogP less than or equal to 3, hydrogen bond donors less than or equal to 3, hydrogen bond acceptors less than or equal to 3, rotatable bonds less than or equal to 3, and polar surface area less than or equal to 60 $Å^2$. Once a fragment library has been prepared, it will be followed by a screening step to identify potential hits. In this study, the predesigned Maybridge Ro3 diversity fragment library, which is composed of 2,500 structurally diverse fragments was downloaded and prepared. The preparation step has resulted in 2,969 different fragments due to ionization, isomerization, and tautomerization of input fragments. Then, the prepared library was converted into a 3D database and was ready for virtual screening.

#### 2.1.2 Screening of Fragment Library

In order to speed up the process of fragments docking and to focus on fragments that are capable of forming desirable interactions with the two specified docking regions, a pharmacophore-based screening step of the 3D fragment database was performed prior to fragment docking. The first defined region within the GLO-I active site is the Zn-hydrophobic region. Therefore, a customized pharmacophoric zinc binding feature (ZBF) [36] was used as a search query using the *Search 3D Database* protocol within DS to identify fragments within the Ro3 library that possess zinc binding groups. This search retained 409 fragment hits. Similarly, in order to identify fragments' complementary to the positively charged mouth, a negative-ionizable (NI) pharmacophoric feature was used and 306 hits were retained (Figure 3). The retained hits were then docked into their corresponding regions.

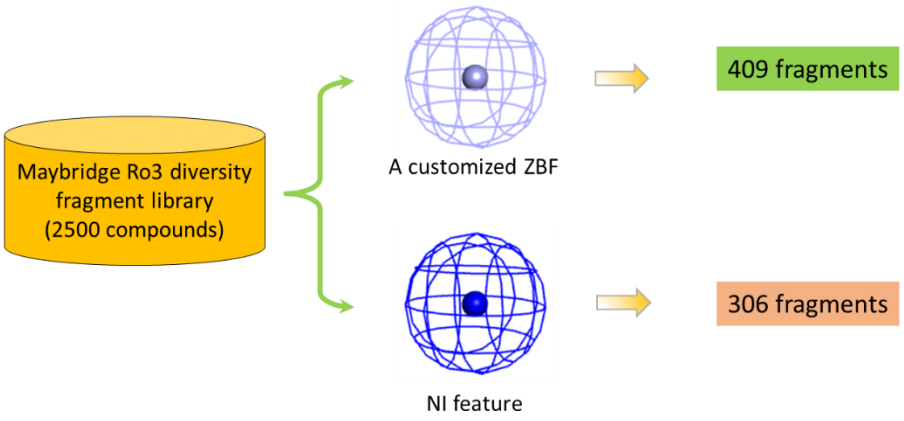


**Figure 3:** Primary screening of the Maybridge Ro3 database using a customized zinc binding and a negatively ionizablepharmacophoric search queries.

**2.1.3 Fragment Docking and Scoring**

Different docking protocols are available within DS that can be used in FBDD. Those protocols can be grouped into Ludi-based protocols such as *De Novo Receptor*, *De Novo Link*, and *De Novo Evolution* protocols; and the CHARMm-based *MCSS* protocol [28, 37, 38]. Although any of them can be used in a FBDD study, yet, the nature of the active site of the target of interest and the type of effective interactions it forms with a prospective ligand can guide the choice of the most appropriate approach. Based on the nature of the GLO-I active site, mainly the central $Zn^{2+}$ ion and the positively charged mouth, and the important electrostatic interactions a ligand need to establish with them in order to show good binding affinity, the MCSS protocol was used. The scoring function of the MCSS protocol is a force field-based function, i.e. electrostatic and van der Waal interaction energies are summed up to total interaction energy based on which a ligand is scored and ranked, which are the main interaction types that govern ligand binding affinity to the GLO-I enzyme.

The MCSS scores of the 409 docked fragments into the Zn-hydrophobic region ranged from -6.86 to 214.69 Kcal/mol. The top 35% MCSS scored fragments were retained and the alignments of their docked poses were visually inspected and fragments forming favorable interactions with the $Zn^{2+}$ and the hydrophobic pocket were selected. Out of the 409 docked fragments, 92 were selected for further investigation. For the fragments docked into the positively charged region, their MCSS scores ranged from -41.15 to 183.20 Kcal/mol. Similarly, the top 35% MCSS scored fragments were retained and the alignments of their docked poses were inspected and fragments forming favorable interactions with arginines were selected. Out of the 306 docked fragments, 32 were selected for further investigation.

**2.1.4 Calculation of Binding Energies and Ligand Efficiency of Filtered Fragments**

Although the MCSS score is a force field-based and is considered robust, yet, it does not account for solvation/desolvation energy, entropy, or ΔG of binding. Therefore, the more accurate MM-PBSA method [21], embedded within the *Calculate Binding Energy* protocol in DS, was used to estimate the binding energies of docked fragments poses using equation 1.

$$E_{\cdot Binding} = E_{\cdot Complex} - E_{\cdot Ligand} - E_{\cdot Receptor} \text{(Eq. 1)}$$

Moreover, the ligand efficiency (LE) of docked fragments was also calculated using the *Calculate Ligand Efficiency* protocol in DS (equation 2). Ligand efficiency is an attempt to normalize the activity of a compound by its molecular size, thereby; it represents an indirect measure of the number of constituent atoms that participate in interactions with the target protein [32, 33, 39, 40].

$$\text{LE} = \Delta G \,/\, (\text{Number of nonhydrogen atoms}) \quad \text{(Eq. 2)}$$

The binding energies of the 92 selected fragments from the Zn-hydrophobic region were ranging from -11.9881 to 30.5849 Kcal/mol (the more negative the value the tighter the binding), and their ligand efficiency values were ranging from -4.55562 to 3.02026. The binding energies of the 32 selected fragments from the positively charged region were ranging from -46.3394 to 21.8898 Kcal/mol and their ligand efficiency values were ranging from -3.50089 to 1.56356. Hence, a more negative value of LE is favorable since the estimated binding energy of docked fragments is reported as a negative value.

**2.1.5 Selection of Core Fragments**

In order to select the final core fragments that would be used to build the final compounds, further inspection was preformed to select the most suitable ones. The inspection and assessment criteria included the docked pose alignment,

 

MCSS docking score, ligand efficiency, free binding energy, feasibility of chemical synthesis, and fragment commercial availability. Based on these criteria, three core fragments fitting the Zn-hydrophobic region were selected, namely 2-hydroxy-3-phenylpropanoic acid, 2-hydroxy-2-phenylacetic acid, and 2-ethylbenzoic acid (Table 1 and Figure 4). Moreover, three core fragments fitting the positively charged region were selected, namely 2-(4-flourophenylthio)acetic acid, 2-(3-methoxyphenyl)acetic acid, and 4-(trifluoromethyl)nicotinic acid (Table 2 and Figure 5).

**Table 1. The selected fragments binding to the Zn-hydrophobic region.**

| Index | Chemical Structure | Code | MCSS Score | TBE[a] | Ligand Efficiency | M. Wt. |
|---|---|---|---|---|---|---|
| **1A** | 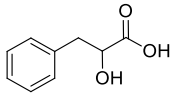 | AC42777 | 156.19 | 10.74 | 0.90 | 166.2 |
| **2A** | 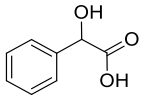 | JFD03933 | 142.13 | -3.59 | -0.33 | 152.2 |
| **3A** | 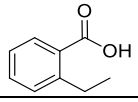 | AC37875 | 127.50 | 0.52 | 0.05 | 150.2 |

[a]Total Binding Energy Kcal/mol

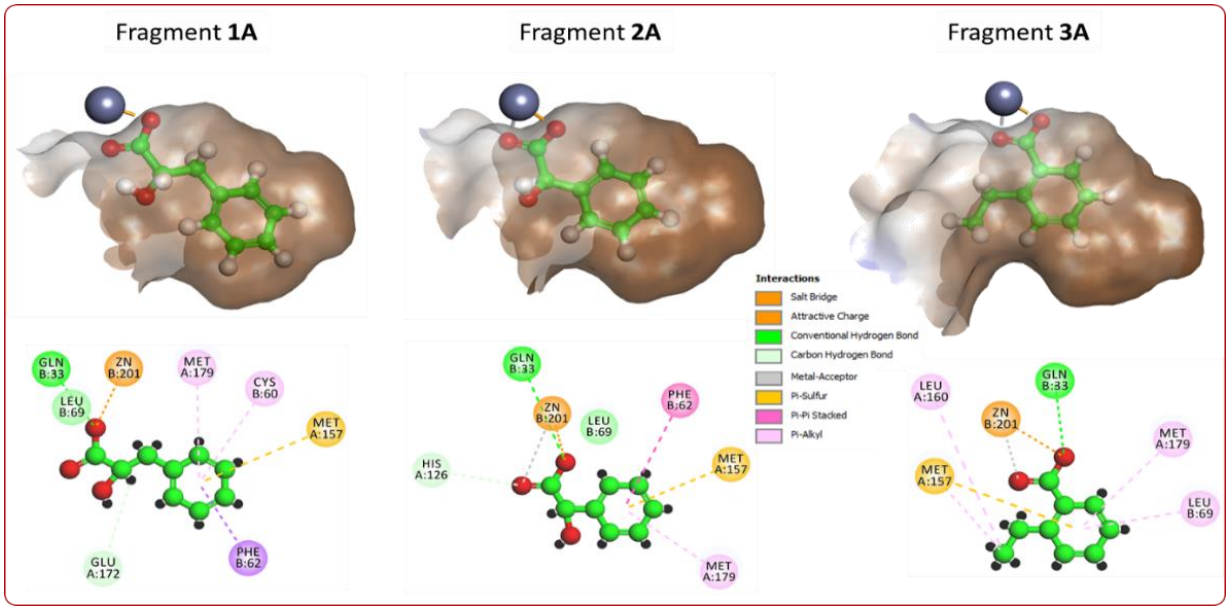


**Figure 4:** Upper panel: the docked poses of the selected fragments binding the Zn-hydrophobic region. The binding site is represented as a hydrophobic surface (brown), the zinc atom as a grey sphere, and the docked fragments in balls and sticks with carbon atoms colored green. Lower panel: 2D interaction map of the docked fragments with amino acid residues within the binding region.

**Table 2.The selected core fragments binding the positively charged region.**

| Index | Chemical Structure | Code | MCSS Score | TBE[a] | Ligand Efficiency | M. Wt. |
|---|---|---|---|---|---|---|
| **1B** | 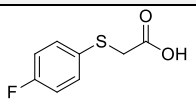 | KM09206 | 104.72 | -33.09 | -2.76 | 185.0 |
| **2B** | 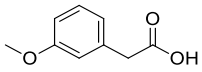 | BTB09242 | 99.48 | -35.62 | -2.97 | 165.1 |
| **3B** | 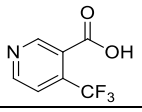 | RF03948 | 106.44 | -29.37 | -2.26 | 190.0 |

[a]Total Binding Energy Kcal/mol

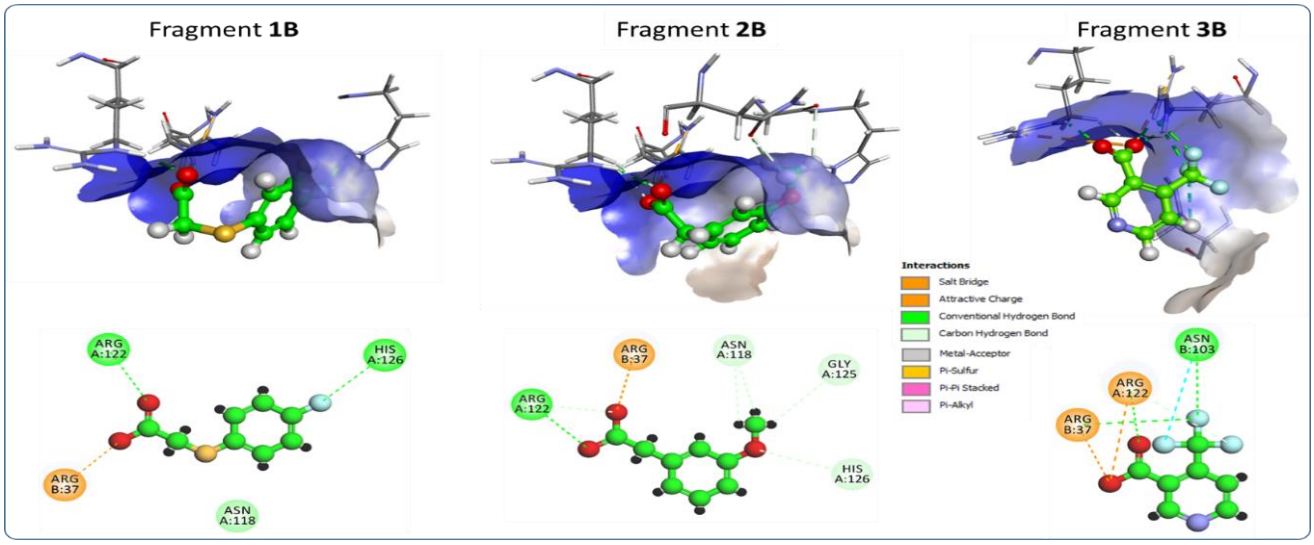


**Figure 5:** Upper panel: docked poses of the selected fragments binding the positively charged region. The binding site is represented as a hydrophobic surface (blue), and the docked fragments in balls and sticks with carbon atoms colored green. Lower panel: 2D interaction map of the docked fragments with amino acid residues within the binding region.

Moreover, from a chemical synthetic point of view, the selected fragments need to have reactive handles, functional groups, such that the synthesis of final compounds would be feasible. Therefore, analogs for the selected fragments that possess functionalities deemed important for feasible synthesis of the final evoluted compounds were selected (Table 3).

**Table 3. The selected core fragments binding the positively charged region and the Zn-hydrophobic regions along with their respective functionalized analogs.**

| Index | Selected fragment | Analog fragment |
|---|---|---|
| **Core fragments binding the Zn-hydrophobic region** | | |
| **1A** | 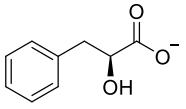 2-hydroxy-3-phenylpropanoic acid | 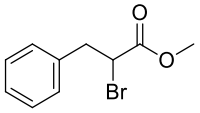 Methyl 2-bromo-3-phenylpropanoate |
| **2A** | 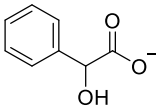 2-hydroxy-2-phenylacetic acid | 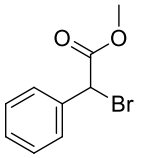 Methyl 2-bromo-2-phenylacetate |
| **3A** | 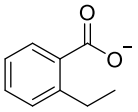 2-ethylbenzoic acid | 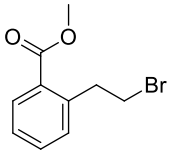 Methyl 2-(2-bromoethyl)benzoate |
| **Core fragments binding the positively charged region** | | |
| **1B** | 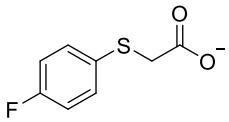 2-(phenylthio)acetic acid | 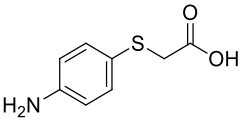 2-((4-aminophenyl)thio)acetic acid |
| **2B** | 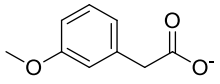 2-(3-methoxyphenyl)acetic acid | 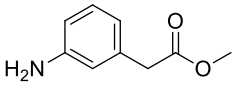 Methyl 2-(3-aminophenyl)acetat |
| **3B** | 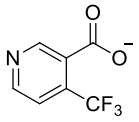 4-(trifluoromethyl)nicotinic acid | 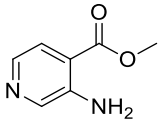 Methyl 3-aminoisonicotinate |

**Fragment Evolution**

The functionalized analogs of the selected core fragments were evoluted towards generating the final putative drug-like compounds using all possible combinations between the two sets of fragments. The evolution step was performed using two strategies, fragment linking and fragment merging. In cases where the fragment binding the positively charged region was overlapping with that binding the Zn-hydrophobic region, fragment-merging approach was used. Fragment **1B** (Table 3) that bind the positively charged region was merged with fragments number **1A**, **2A** and **3A** (Table 3) that bind the Zn-hydrophobic region and led to the generation of final compounds **10**, **16** and **18** (Table 4). An example of this approach is presented in figure 6A, which shows how fragment **1B** was merged with

fragment **1A** to give compound **10**.On the other hand, the fragment linking approach, using a suitable linker, was applied to small fragments that are not overlapping. Fragments **2B** and **3B** were linked to Zn-hydrophobic binding fragments (**1A**, **2A**, and **3A**) using suitable linkers to generate compounds **1-9, 11-15, 17,** and **19-21** (Table 4). Compound **12** is an example of this strategy where fragments **3B** and **2A** were linked together as illustrated in figure 6B.

The selection of suitable linkers was guided by the distance between the reactive handles of the two fragments and the nature of the amino acid residues within the binding site separating those fragments. Hydrophobic aromatic linkers such as 3-nitrobenzenesulfonyl chloride and 3-nitrobenzoyl chloride were selected since the tunnel separating the two regions is composed mainly of aromatic amino acids including Phe162 A, Phe67B, Trp170A, and Met35B. Using flexible linkers such as propyl and butyl linkers led to mostly unfavorable and less stable binding modes as inferred from docking such compounds.

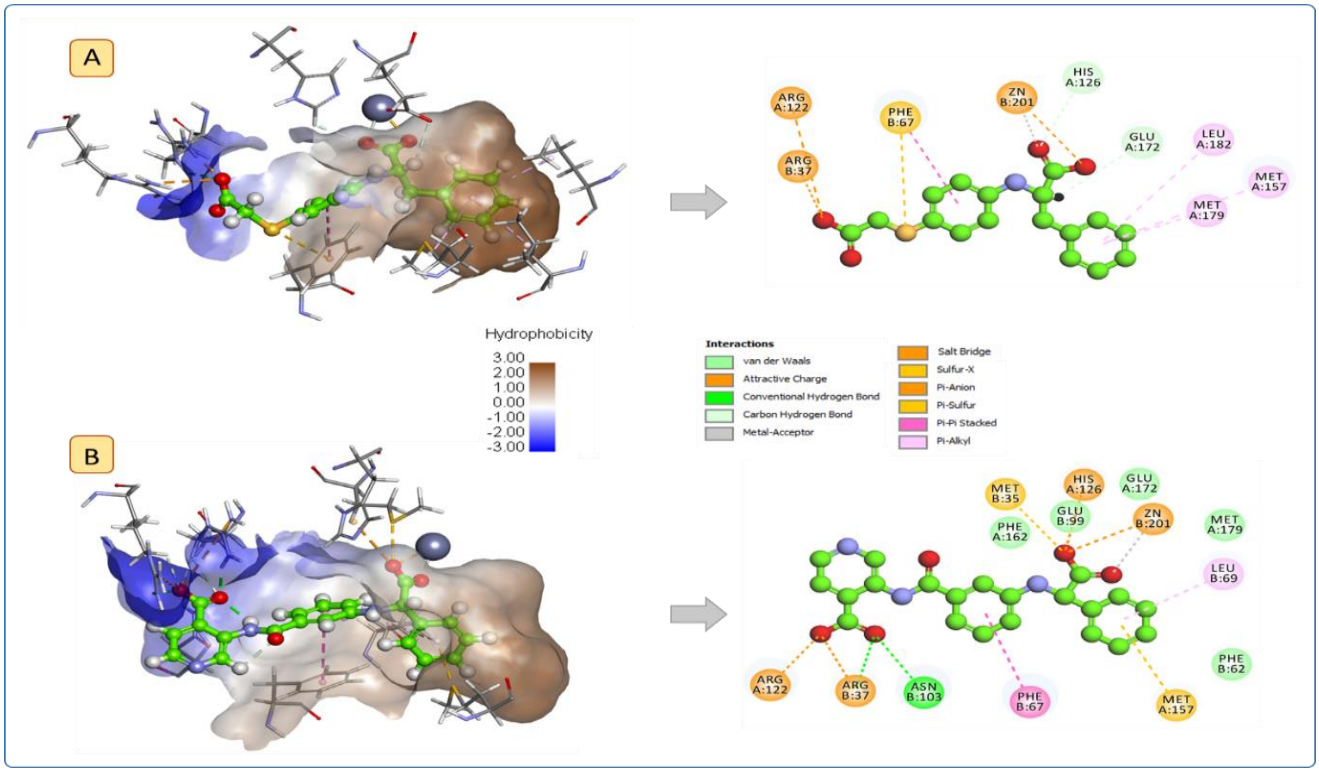


**Figure 6**: (A) The top ranked docked pose of compound 10, which is an example of fragments merging approach, into the active site of GLO-I along with a 2D interaction map showing the essential interaction it forms with the enzyme. (B) The top ranked docked pose and the 2D interaction map of compound 12 which is an example of fragments linking approach. Residues are colored according to the type of their interactions with the ligand. The binding site is represented as a hydrophobic surface (blue is positively charged areas and brown is hydrophobic areas), docked compounds are shown in balls and sticks with carbons colored green, and Zn atom as a grey sphere.

**2.1.6 Molecular Docking and Calculation of Binding Energy of Evoluted Compounds**

Prior to molecular docking of the final evoluted compounds, the GLO-I active site was defined by a sphere of 13 Å radius based on the complexed ligand in the downloaded crystal structure. Then the evoluted final compounds were docked using the *CDOCKER Docking* protocol. The generated poses of the docked compounds were ranked based on -CDOCKER energy, which corresponds to ligand-receptor interaction energy plus ligand strain; and the -CDOCKER interaction energy, which corresponds to ligand-receptor interaction energy; where higher values correspond to better binding affinity. The -CDOCKER energy scores were ranging from 44.4002 to 68.6103Kcal/mol. Afterwards, the binding energies of docked poses were calculated using the MM-PBSA implicit solvent model in order to account for the solvation/ desolvation energy, entropy, or ΔG of binding that are missing in the CDOCKER scores. The binding energy values of docked poses were ranging from -41.1874 to 8.7012 Kcal/mol (Table 4).

Accounting for the flexibility of amino acid residues within the binding site allows greater realism than other docking formalisms, thereby, adding to the accuracy of the docking scores. Therefore, a new cycle of docking was initiated using the *Flexible Docking* protocol in DS. Ranking of the docked compounds was based on the empirical Libdock score, which is a Piecewise Linear Potential (PLP) like score (steric and H-bonding intermolecular functions) where higher PLP scores indicate stronger binding affinity [41]. The libdock scores of the evoluted compounds were ranging from 82.4295 to 116.98 Kcal/mol (Table 4).

**Table 4. List of all possible evoluted final compounds sorted in a decreasing order of their Libdock score.**

| No. | Chemical structure | Libdock score | M. wt. | CDOCKER | | |
|---|---|---|---|---|---|---|
| | | | | - CDIE[a] | -CDE[b] | BE[c] |
| 1 | 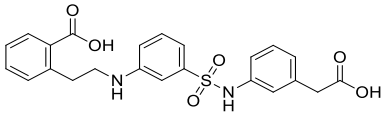 | 116.98 | 452.48 | 61.45 | 49.20 | -22.68 |
| 2 | 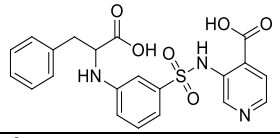 | 112.20 | 438.45 | 73.40 | 62.40 | -13.05 |
| 3 | 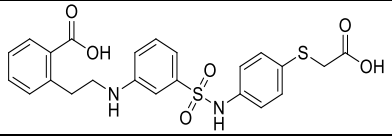 | 108.43 | 498.59 | 58.95 | 48.00 | -25.51 |
| 4 | 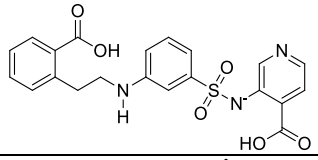 | 103.43 | 438.43 | 58.39 | 47.42 | -13.08 |
| 5 | 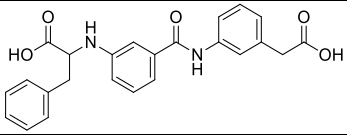 | 103.40 | 416.14 | 70.49 | 63.53 | -4.44 |

| No. | Chemical structure | Libdock score | M. wt. | CDOCKER | | |
|---|---|---|---|---|---|---|
| | | | | - CDIE[a] | -CDE[b] | BE[c] |
| 6 | 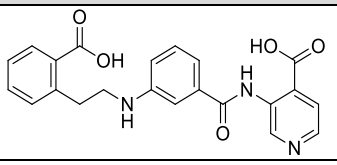 | 100.05 | 403.40 | 51.35 | 42.50 | -13.68 |
| 7 | 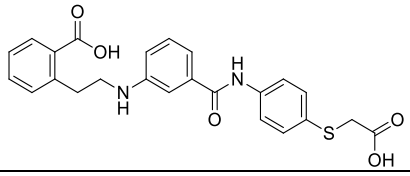 | 98.60 | 462.53 | 60.43 | 44.24 | -31.55 |
| 8 | 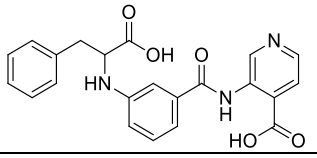 | 97.73 | 403.40 | 61.40 | 51.44 | 0.10 |
| 9 | 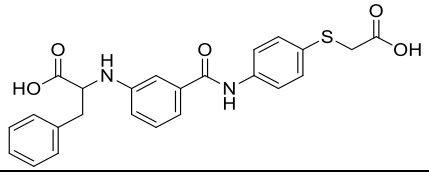 | 96.91 | 448.11 | 71.53 | 60.28 | -13.81 |
| 10 | 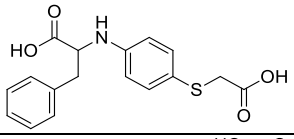 | 96.32 | 329.07 | 64.97 | 57.70 | -22.68 |
| 11 | 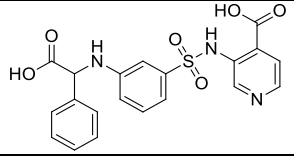 | 96.15 | 424.42 | 60.75 | 53.69 | -24.35 |
| 12 | 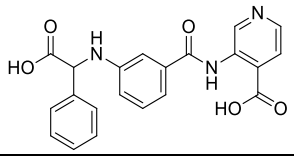 | 96.15 | 391.37 | 65.43 | 49.37 | 4.26 |
| 13 | 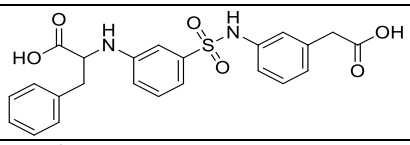 | 95.94 | 452.10 | 74.40 | 62.88 | -27.54 |
| 14 | 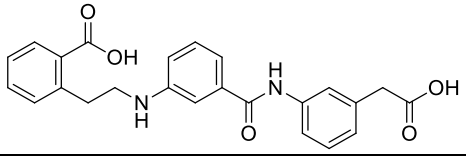 | 94.64 | 416.44 | 58.05 | 44.76 | -7.54 |

| No. | Chemical structure | Libdock score | M. wt. | CDOCKER | | |
|---|---|---|---|---|---|---|
| | | | | - CDIE[a] | -CDE[b] | BE[c] |
| 15 | 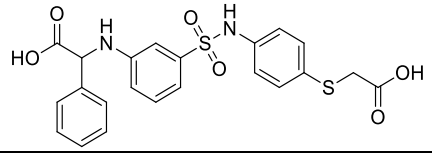 | 91.39 | 470.06 | 68.91 | 57.69 | -1.54 |
| 16 | 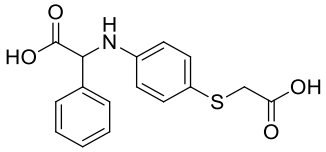 | 90.12 | 315.06 | 61.77 | 53.85 | -22.07 |
| 17 | 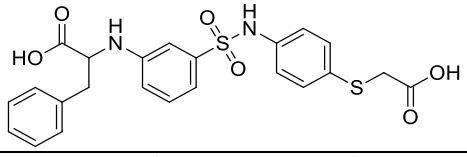 | 88.77 | 484.08 | 68.09 | 57.20 | 1.60 |
| 18 | 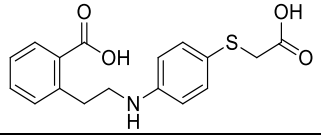 | 87.12 | 344.42 | 53.06 | 59.72 | -17.80 |
| 19 | 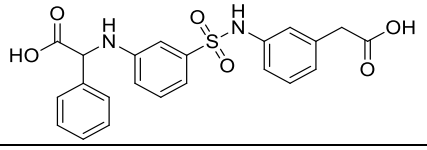 | 86.82 | 438.09 | 68.85 | 59.96 | -15.20 |
| 20 | 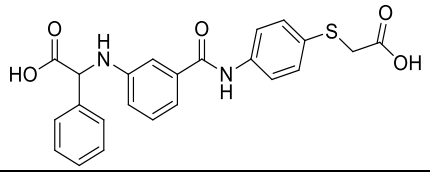 | 83.20 | 434.09 | 68.85 | 51.58 | 8.70 |
| 21 | 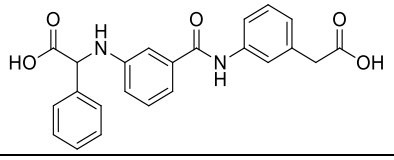 | 83.19 | 402.12 | 65.60 | 55.74 | -27.72 |

[a]: The negative value of CDOCKER interaction energy.
[b]: The negative value of CDOCKER energy.
[c]: The free binding energy.

### 2.2 *Synthesis*

In order to assess the applicability of our approach, one of the final evoluted compounds was synthesized (compound **12** in table 4). This compound was chosen as a pilot compound because it showed a Libdock score midway between the minimum and maximum score values. Accordingly, its measured activity can be extrapolated to get a rough estimate of the activities of other compounds within the evoluted set.

In general, the synthesis of compound **12** was accomplished via four synthetic steps as illustrated in scheme 1. The first step was the coupling of the arginine-binding fragment, methyl 3-aminoisonicotinate (fragment **3B** analog), with the 3-nitrobenzoyl chloride linker. Then,

the nitro group of the linker was reduced into an amine to which the Zn-binding fragment, methyl 2-bromo-2-phenylacetate (fragment **2A** analog), was coupled. Finally, hydrolysis of the ester functionalities resulted in the final desired compound.

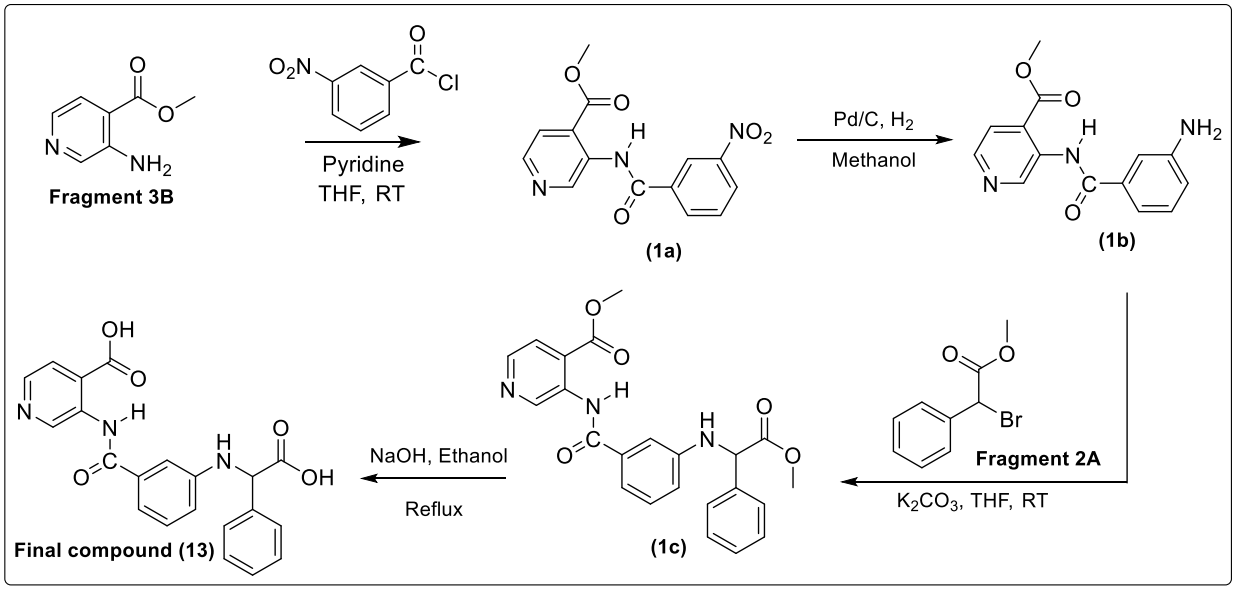


**Scheme 1: The synthetic scheme of compound 12.**

Specifically, methyl 3-(3-nitrobenzamido)isonicotinate (**1a**) was prepared by stirring one equivalent of triethylamine (TEA), one equivalent of methyl 3-aminoisonicotinate (fragment **3B** analog) and one equivalent of 3-nitrobenzoyl chloride in anhydrous THF for 7 h at rt. Then the reaction mixture was poured into acidic water where the product was precipitated, collected, and then dried. The product was found to be of enough purity as inferred from its $^{1}$H-NMR spectrum. Therefore, it was used as is in the next step without further purifications.

Methyl 3-(3-aminobenzamido)isonicotinate (**1b**) was prepared by stirring compound **1a** with Pd/C and $H_2$ overnight at room temperature. Then, Pd/C was discarded by suction filtration and the filtrate was evaporated to collect the product which was then recrystallized from ethyl acetate and hexane. Later, methyl 3-(3-((2-methoxy-2-oxo-1-phenylethyl)amino)benzamido)isonicotinate (**1c**) was prepared by stirring one equivalent of potassium carbonate, one equivalent of compound **1b**, and one equivalent of methyl 2-bromo-2-phenylacetate (fragment **2A** analog) in anhydrous THF overnight at rt. Upon completion of the reaction, the reaction mixture was poured into ice water and left in the fridge overnight, then the precipitated product was collected, dried, and recrystallized from ethyl acetate and hexane. The final compound, **12,** was prepared by dissolving compound **1c** in a basic solution of 0.3 mM of sodium hydroxide and ethanol, and after completion of the reaction it was acidified to pH 3 and the precipitated product was collected and recrystallized from methanol and dichloromethane.

The identity of intermediate compounds was confirmed using $^{1}$H and $^{13}$C-NMR data, except for compound **1b**, in which the reduction of the nitro functionality into an amine was verified using IR. The final compound (**12**) was fully characterized using $^{1}$H and $^{13}$C-NMR, HRESIMS, and IR spectroscopy (Figures S1-S7).

### 2.3 *In vitro enzyme assay*

The *in vitro* inhibitory activity of the synthesized compound against GLO-I was performed using the human recombinant GLO-I enzyme (rhGLO-I). Generally, when the GLO-I interacts with its substrate, hemithioacetal, S-D-lactoylglutathione starts forming. The formation of S-D-lactoylglutathione can be measured spectrophotometrically by monitoring the increase in absorbance at 240 nm. The absorbance was plotted versus time and the slope was calculated, then the percent of GLO-I inhibition was calculated using equation 3 and compared to myricetin which was used as a positive control. The percent of GLO-I inhibition by compound **12** and myricetin at 50 $\mu$M was calculated in three independent experiments.

$$\% \; inhibition = 1 - \frac{slope \; of \; the \; tested \; compound}{slope \; of \; the \; negative \; control} \; x \; 100\% \quad \text{(Eq. 3)}$$

The percent of GLO-I inhibition by compound **12** was 43.93% ±6.00,which is one fold lower than that of myricetin that was 86.13% ±2.71. Although the activity of **12** is moderate, yet, synthesis of only one compound out of the proposed 21 with a percent of inhibition of 43.93 at 50 $\mu$M gives an indication that our approach seems to be successful. Since compound **12** is not the top-ranked in the series, probably, synthesis of all evoluted compounds could have resulted in better results upon which solid conclusions can be drawn. Figure 7 summarizes the overall approach implemented in this work.

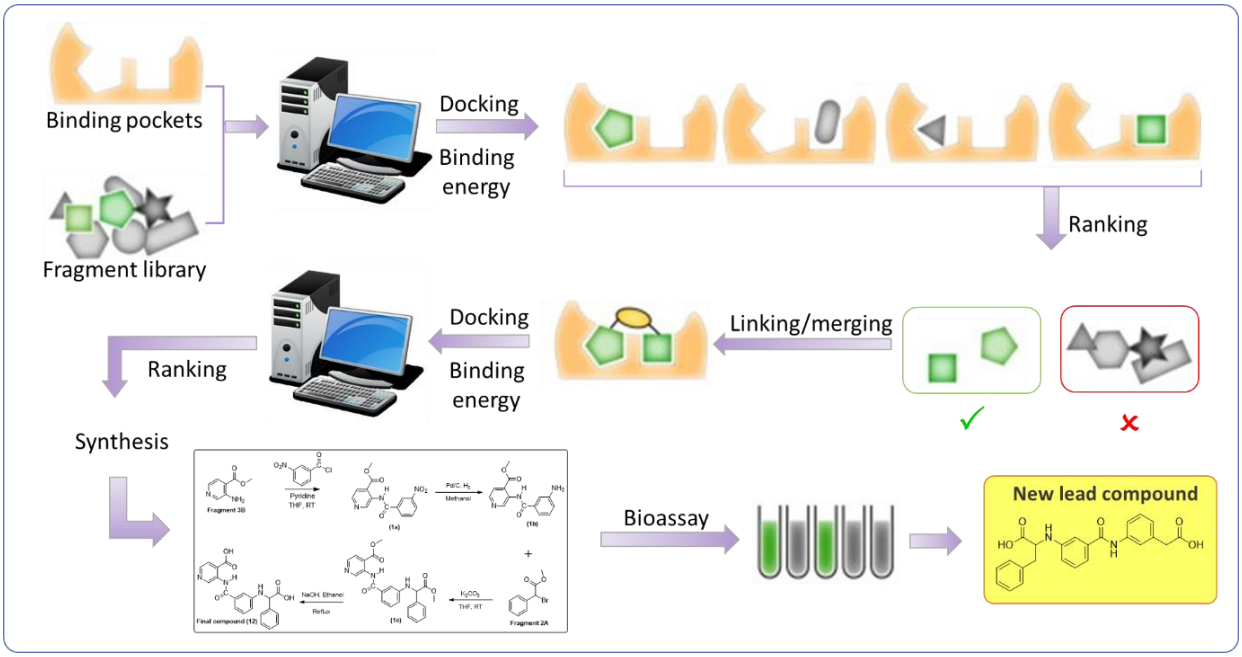


**Figure 7: Summary of the overall approach implemented in this study.**

## CONCLUSION

In conclusion, a computational fragment-based drug design approach was employed in this study to design potential GLO-I inhibitors. The approach was based on screening the Maybridge Ro3 diversity fragment library using different computational techniques in order to select potential fragments that could be evoluted to obtain drug-like active compounds. Six fragments were selected that are

complementary to the main binding regions within the GLO-I active site. Fragments merging and linking had resulted in 21 potential GLO-I inhibitors. However, due to the synthetic constrains associated with fragment-based design, only one compound (**12**) was synthesized and biologically evaluated. This compound was chosen as a pilot compound to assess the validity of our approach because it showed a Libdock score, compared to other proposed compounds, midway between the minimum and maximum score values. The percent of GLO-I inhibition at 50 $\mu$M of compound **12** was 44% indicating the success of the utilized approach. Despite the moderate activity, the percent of inhibition of compound **12** can be extrapolated to get a rough estimate of the expected activities of other compounds within the evoluted set. This compound could be considered as a new hit with a novel scaffold that can be further optimized towards designing more potent GLO-I inhibitors.

## CONFLICT OF INTEREST

Authors declare no conflict of interest.

## ACKNOWLEDGEMENT

The authors wish to thank the Deanship of Scientific Research at Jordan University of Science and Technology for financial support, grant number (20170238). The high-resolution mass spectrometry data were acquired in the Triad Mass Spectrometry Laboratory at the University of North Carolina at Greensboro.

## REFERENCES

(1) Racker E. The mechanism of action of glyoxalase. *Journal of Biological Chemistry*. 1951; 190:685-696.

(2) Thornalley P. J. The glyoxalase system in health and disease. *Molecular aspects of medicine*. 1993; 14:287-371.

(3) Inoue Y. and A. Kimura. Methylglyoxal and regulation of its metabolism in microorganisms. *Advances in microbial physiology*. 1995; 37:177-227.

(4) Thornalley P. J. Advances in glyoxalase research. Glyoxalase expression in malignancy, anti-proliferative effects of methylglyoxal, glyoxalase I inhibitor diesters and S-d-lactoylglutathione, and methylglyoxal-modified protein binding and endocytosis by the advanced glycation endproduct receptor. *Critical Reviews in Oncology/Hematology*. 1995; 20:99-128.

(5) Samadi A. A., S. A. Fullerton ,D. G. Tortorelis, G. B. Johnson, S. D. Davidson, M. S. Choudhury, C. Mallouh, H. Tazaki, and S. Konno. Glyoxalase I phenotype as a potential risk factor for prostate carcinoma. *Urology*. 2001; 57:183-187.

(6) Papaconstantinou J. and S. P. Colowick. The Role of Glycolysis in the Growth of Tumor Cells II. The effect of oxamic acid on the growth of hela cells in tissue culture. *Journal of Biological Chemistry*. 1961; 236:285-288.

(7) Sakamoto H., T. Mashima, S. Sato, Y. Hashimoto, T. Yamori, and T. Tsuruo .Selective activation of apoptosis program by Sp-bromobenzylglutathione cyclopentyl diester in glyoxalase I-overexpressing human lung cancer cells. *Clinical cancer research*. 2001; 7:2513-2518.

(8) Jones M. B., H. Krutzsch, H. Shu, Y. Zhao, L. A. Liotta, E .C. Kohn, and E. F. Petricoin. Proteomic analysis and identification of new biomarkers and therapeutic targets for invasive ovarian cancer. *Proteomics*. 2002; 2:76-84.

(9) Vince R., S. Daluge, and W. B. Wadd. Inhibition of glyoxalase I by S-substituted glutathiones. *Journal of medicinal chemistry*. 1971; 14:402-404.

(10) More S. S. and R. Vince. A metabolically stable tight-binding transition-state inhibitor of glyoxalase-I. *Bioorganic & Medicinal Chemistry Letters*. 2006; 16:6039-6042.

(11) More S. S. and R. Vince. Design, synthesis, and binding

studies of bidentate Zn-chelating peptidic inhibitors of glyoxalase-I. *Bioorganic & medicinal chemistry letters*. 2007; 17:3793-3797.

(12) Jordan F., J. f. Cohen, C.-T. Wang, J. m. Wilmott, S. s. Hall, and D. l .Foxall. Glyoxalase I: Mechanism-Based Inhibitors. *Drug Metabolism Reviews*. 1983; 14:723-740.

(13) Al-Balas Q., M. Hassan, B. Al-Oudat, H. Alzoubi, N. Mhaidat, and A. Almaaytah. Generation of the first structure-based pharmacophore model containing a selective "zinc binding group" feature to identify potential glyoxalase-1 inhibitors. *Molecules*. 2012; 17:13740-13758.

(14) Al-Balas Q. A., M. A. Hassan, N. A. Al-Shar'i, N. M. Mhaidat, A. M. Almaaytah, F. M. Al-Mahasneh, and I. H. Isawi. Novel glyoxalase-Iinhibitors possessing a "zinc-binding feature" as potential anticancer agents. *Drug design, development and therapy*. 2016; 10:2623.

(15) Al-Balas Q., M. Hassan, G. Al-Jabal, N. Al-Shar'i, A. Almaaytahb, and T. Elimata. Novel Thiazole Carboxylic Acid Derivatives Possessing a "Zinc Binding Feature" as Potential Human Glyoxalase-I Inhibitors. *Letters in Drug Design & Discovery*. 2017; 14:1324-1334.

(16) Thornalley P. J. Glyoxalase I – structure, function and a critical role in the enzymatic defence againstglycation. *Biochemical Society Transactions*. 2003; 31:1343-1348.

(17) Cameron A. D., M. Ridderström, B. Olin, M. J. Kavarana, D. J. Creighton, and B. Mannervik. Reaction Mechanism of Glyoxalase I Explored by an X-ray Crystallographic Analysis of the Human Enzyme in Complex with a Transition State Analogue. *Biochemistry*. 1999; 38:13480-13490.

(18) Cameron A. D., B. Olin, M. Ridderström, B. Mannervik, and T. A. Jones. Crystal structure of human glyoxalase I—evidence for gene duplication and 3D domain swapping. *The EMBO Journal*. 1997; 16:3386-3395.

(19) Al-Balas Q. A., N. Al-Shar'i, K. Banisalman, M. Hassan, G. A. Jabal, and A. Almaaytah. Design, Synthesis and Biological Evaluation of Potential Novel Zinc Binders Targeting Human Glyoxalase-I; A ValidatedTarget for Cancer Treatment *Jordan Journal of Pharmaceutical Sciences*. 2018; 11:25-37.

(20) Discovery Studio. 2017, Accelrys Inc.: San Diego, CA, USA.

(21) Genheden S. and U. Ryde. The MM/PBSA and MM/GBSA methods to estimate ligand-binding affinities . *Expert opinion on drug discovery*. 2015; 10:449-461.

(22) The Maybridge Ro3 2500 Diversity Fragment Library, 2017, Maybridge, part of Thermo Fisher Scientific

(23) Nguyen D. X. and J. Massague. Genetic determinants of cancer metastasis. *Nature Reviews Genetics*. 2007; 8:341-352.

(24) Calculation and plotting of the % enzyme inhibition, GraphPad Prism version 6.01 for Windows. p. GraphPad Software, La Jolla California USA, www.graphpad.com.

(25) Brooks B. R., C. L. Brooks, A. D. MacKerell, L. Nilsson, R .J. Petrella, B. Roux, Y. Won, G. Archontis, C. Bartels, S. Boresch, A. Caflisch, L. Caves, Q. Cui, A. R. Dinner, M. Feig, S. Fischer, J. Gao, M. Hodoscek, W. Im, K. Kuczera, T. Lazaridis, J. Ma, V. Ovchinnikov, E. Paci, R. W. Pastor, C. B. Post, J. Z. Pu, M. Schaefer, B. Tidor, R. M. Venable, H. L. Woodcock, X. Wu, W. Yang, D. M. York, and M. Karplus. CHARMM: The Biomolecular Simulation Program. *Journal of Computational Chemistry*. 2009; 30:1545-1614.

(26) Hecker E. A., C. Duraiswami, T. A. Andrea, andD. J. Diller. Use of Catalyst Pharmacophore Models for Screening of Large Combinatorial Libraries. *Journal of Chemical Information and Computer Sciences*. 2002; 42:1204-1211.

(27) Osman G., C. Omoshile, and K. Yasuhisa. Pharmacophore Modeling and Three Dimensional Database Searching for Drug Design Using Catalyst: Recent Advances. *Current*

*Medicinal Chemistry*. 2004; 11:2991-3005.

(28) Miranker A. and M. Karplus. Functionality maps of binding sites: a multiple copy simultaneous search method. *Proteins: Structure, Function, and Bioinformatics*. 1991; 11:29-34.

(29) Tirado-Rives J. and W. L. Jorgensen. Contribution of Conformer Focusing to the Uncertainty in Predicting Free Energies for Protein−Ligand Binding. *Journal of medicinal chemistry*. 2006; 49:5880-5884.

(30) Hilderbrandt R. L. Application of Newton-Raphson optimization techniques in molecular mechanics calculations. *Computers and Chemistry*. 1977; 1:179-186.

(31) Hunter D. R. and K. Lange. A Tutorial on MM Algorithms. *The American Statistician*. 2004; 58:30-37.

(32) Reynolds C. H., B. A. Tounge, and S. D. Bembenek. Ligand binding efficiency: trends, physical basis, and implications. *Journal of medicinal chemistry*. 2008; 51:2432-2438.

(33) Congreve M., G. Chessari, D. Tisi, and A. J. Woodhead. Recent developments in fragment-based drug discovery. *Journal of medicinal chemistry*. 2008; 51:3661-3680.

(34) Beligny S. and J. Rademann, Oxidizing and reducing agents, in The Power of Functional Resins in Organic Synthesis. 2009, Wiley.

(35) Muegge I. PMFScoring Revisited. *Journal of Medicinal Chemistry*. 2006; 49:5895-5902.

(36) Al-Shar'i N. A., M. Hassan, Q. Al-Balas, and A. Almaaytah. Identification of Possible Glyoxalase II Inhibitors as Anticancer Agents by a Customized 3D Structure-Based Pharmacophore Model. *Jordan Journal of Pharmaceutical Sciences*. 2015; 8.

(37) Böhm H.-J. LUDI: rule-based automatic design of new substituents for enzyme inhibitor leads. *Journal of computer-aided molecular design*. 1992; 6:593-606.

(38) Gehlhaar D. K., G. M. Verkhivker, P. A. Rejto, C. J. Sherman, D. B. Fogel, L. J. Fogel, and S. T. Freer. Molecular recognition of the inhibitor AG-1343 by HIV-1 protease: conformationally flexible docking by evolutionary programming. *Chemistry and Biology*. 1995; 2:317-324.

(39) Hopkins A. L., C. R. Groom, and A. Alex. Ligand efficiency: a useful metric for lead selection. *Drug discovery today*. 2004; 9:430-431.

(40) Schultes S., C. de Graaf, E. E. Haaksma, I. J. de Esch, R. Leurs, and O. Krämer. Ligand efficiency as a guide in fragment hit selection and optimization. *Drug Discovery Today: Technologies*. 2010; 7:e157-e162.

(41) Sousa Silva M., Ricardo A. Gomes, Antonio E. N. Ferreira, A. Ponces Freire, and C. Cordeiro. The glyoxalase pathway: the first hundred years… and beyond. *Biochemical Journal*. 2013; 453:1-15.

# اكتشاف مثبطات جديدة لأنزيم الجلايوكسيليز-1 باستخدام نهج تصميم الدواء المعتمد على المركبات الكيميائية الصغيرة

**نزار الشرع[1]، محمد حسان[1]، هديل البرقي[1]، قصي البلص[1]، تمام العليمات[1]***

**1- قسم الكيمياء الطبية والعقاقير، كلية الصيدلة، جامعة العلوم والتكنولوجيا ،الاردن**

## ملخص

أستخدم في هذه الدراسة نهج تصميم الدواء المعتمد على المركبات الكيميائية الصغيرة، لتصميم مثبطات محتملة لأنزيم الجلايوكسيليز-1. يحدث فرط في إنتاج هذا الانزيم في أنواع مختلفة من السرطان، مما جعله هدفاً عملياً لعلاج السرطان. استند النهج الحالي إلى فحص قاعدة بيانات Maybridge Ro3 للمركبات الصغيرة باستخدام تقنيات حسابية مختلفة لتحديد المركبات الصغيرة المحتملة التي يمكن تطويرها إلى مركبات فعالة. اختيرت ستة مركبات صغيرة ترتبط بشكل تكاملي في مناطق الربط الرئيسة داخل موقع الإنزيم النشط. نتج عن دمج وربط هذه المركبات الصغيرة ببعضها 21 مركباً محتملا لتثبيط إنزيم الجلايوكسيليز-1. لتقييم مدى قابلية تطبيق هذا النهج، تم تصنيع مركب تجريبي واحد (مركب رقم 12) وتقييمه بيولوجياً. حيث كانت نسبة تثبيط الانزيم44% باستخدام تركيز 50 ميكرومولر، أقل بمقدار الضعف عن الميريسيتين (86٪)، مما يشير إلى نجاح النهج المستخدم في هذه الدراسة. على الرغم من الفعالية المتوسطة للمركب المصنع،إلا أنه يمكن استخدامه للإستقراء وللحصول على تقدير تقريبي للفاعلية المتوقعة للمركبات الأخرى ضمن المجموعة المطورة. علاوة على ذلك،للمركب 12 تركيب كيميائي بنمط جديد، حيث يمكن إجراء العديد من التحسينات عليه لتصميم مثبطات أكثر فاعلية لهذا الإنزيم.

**الكلمات الدالة:**الجلايوكسيليز-1، تصميم الأدوية باستخدام المركبات الكيميائية الصغيرة، الربط مع الزنك، مضاد للسرطان.

---

تاريخ استلام البحث2019/3/31 وتاريخ قبوله للنشر 2019/7/8.